Wavenumber prediction and measurement of axisymmetric waves in buried fluid-filled pipes: inclusion of shear coupling at the pipe/soil interface

J. M. Muggleton[a]* & J. Yan[b]

[a] *Institute of Sound and Vibration Research, Southampton University, Highfield, Southampton SO17 1BJ, England*

[b] *Engineering College, Guangdong Ocean University, Zhanjiang 524088, China*

Abstract: Acoustic methods have been widely used to detect water leaks in buried fluid-filled pipes, and these technologies also have the potential to locate buried pipes and cables. Relatively predictable for metal pipes, there is considerably more uncertainty with plastic pipes, as the wave propagation behaviour becomes highly coupled between the pipe wall, the contained fluid and surrounding medium. Based on the fully three-dimensional effect of the surrounding soil, pipe equations for n=0 axisymmetric wave motion are derived for a buried, fluid-filled pipe. The characteristics of propagation and attenuation are analyzed for two n=0 waves, the s=1 wave and s=2 wave, which correspond to a predominantly fluid-borne wave and a compressional wave predominantly in the shell, respectively. At the pipe/soil interface, two extreme cases may be considered in order to investigate the effects of shear coupling: the "slip" condition representing lubricated contact; and the "no slip" condition representing compact contact. Here, the "slip" case is considered, for which, at low frequencies, analytical expressions can be derived for the two wavenumbers, corresponding to the s=1 and s=2 waves. These are both then compared with the situations in which there is no surrounding soil and in which the pipe is surrounded by

fluid only, which cannot support shear. It is found that the predominant effect of shear at the pipe/soil interface is to add stiffness along with damping due to radiation. For the fluid-dominated wave, this causes the wavespeed to increase and increases the wave attenuation. For the shell-dominated wave there is little effect on the wavespeed but a marked increase in wave attenuation. Comparison with experimental measurements confirm the theoretical findings.

Key words: Buried fluid-filled pipes, Wavenumber, Pipe/soil shear coupling, Propagation, Attenuation

***** Corresponding author. *E-mail address*: jm9@soton.ac.uk (J. M. Muggleton)

1. Introduction

Water leakage from buried pipes is a subject of increasing concern because of decreasing water supplies and the deterioration of old pipework. Since the loss of large amounts of water through leak pipework system is both environmentally and economically damaging, much attention has been paid to reducing water leakage over the past few years. Meanwhile, the problems associated with inaccurate location of buried pipes and cables have been very serious for many years and are getting worse as a result of increasing traffic congestion in the worldwide major urban areas. A recent UK study estimated that streetworks cost the UK £7bn in lost revenues annually; comprising £5.5bn in social costs and £1.5bn in direct damages [1]. (McMahon et al, 2005).In response to these, a large multi-centre program, Mapping the Underworld [2], is being undertaken in the UK to assess the feasibility of a range of potential technologies that can be combined into a single device to accurately locate buried pipes and cables. An essential technology to be combined into the device is low-frequency vibro-acoustics, and suitable techniques for detecting buried infrastructure, in particular buried plastic water pipes, have been proposed [3] and are currently being developed [4,5].

Detection of water leaks in buried distribution pipes using acoustic methods is common practice in many countries. A leak from a water supply pipe generates noise, which can be used for leak detection and location. Among the various acoustic detection methods, the correlation technique has been proved to be effective for leak detection, which measures acoustic signals at two locations along the pipe, the leak position is then identified by the delay between the leak noise reaching each monitoring point [6]. Although the correlation technique has been successful for many years when used with metal pipes, it remains problematic when used with plastic

pipes. Relatively predictable for metal pipes, there is considerably more uncertainty in the wave propagation parameters with plastic pipes because of their flexibility and the concomitant attenuation. The wave propagation behavior becomes highly coupled between the pipe wall, the contained fluid and surrounding medium, hence the pipe may become a more effective energy radiator [7,8].

Since the correlation technique relies on the vibration characteristics of the pipework system, it is worthwhile to study these characteristics before investigating leak detection, as the propagation wavespeed of the leak signals depends on the pipe material, diameter, and pipe wall thickness [7]. The problem of vibration and wave propagation within elastic, fluid-filled pipes has been studied previously in some detail. Pinnington and Briscoe [9] give low-frequency wavenumber expressions for the axisymmetric fluid-dominated and shell-dominated waves respectively and offer physical interpretations of the results. Fuller and Fahy [10] present dispersion curves and energy distributions of free waves in thin walled cylindrical elastic shells filled with fluid. Sinha *et. al*. [11] present numerical dispersion results for a fluid-filled cylindrical shell and a shell surrounded by an infinite fluid. Safaai-Jazi *et. al*. plot dispersion curves for a cylindrical fluid core surrounded by an infinitely thick solid cladding [12], but no pipe is present. Greenspon [13,14] considers axisymmetric vibrations of both thin and thick cylindrical shells surrounded by water.

However, when the pipe is surrounded by an elastic medium, little work is available in the literature, except for some work concerning the dynamic response to seismic excitation [15,16].

A theoretical model of a buried fluid-filled pipe to predict both wavespeed and attenuation has been developed and validated previously by Muggleton et al. [17].

They investigated the axisymmetric wave propagation in a fluid-filled pipe surrounded by soil, and derived approximate wavenumber expressions for the fluid-dominated and shell-dominated waves, and later also gave some experimental results [18]. However, in their work, the shear coupling of the pipe to the surrounding soil was not properly accounted for: the soil was effectively treated as a fluid supporting two different waves, each of which exerted normal pressure on the pipe wall. Liu et al. [19] modelled a buried pipe as a thin cylindrical shell of linear homogeneous isotropic elastic material surrounded by a linear isotropic homogeneous elastic medium of infinite extent, and the forces exerted in the three orthogonal directions on the pipe wall were included. However, they only computed the natural frequencies for a simply supported pipe, and the effect of the surrounding soil on the pipe were not discussed in detail.

Acoustic energy in buried water pipes generated by a leak propagates at relatively low frequencies. Hunaidi [8] has confirmed that most leak noise energy, on simulated but realistic leaks, is concentrated at frequencies below 100Hz on a plastic pipe distribution system. When the coupled dynamic system vibrates at relatively low frequencies, well below the ring frequency of the pipe, four wave types are responsible for most of the energy transfer [9,10]: three axisymmetric waves, $n = 0$; and the $n = 1$ wave, related to beam bending. Of the $n = 0$ waves, the first, termed $s = 1$, is a predominantly fluid-borne wave; the second wave, $s = 2$ is predominantly a compressional wave in the shell; the third wave, $s = 0$ is a torsional wave uncoupled from the fluid.

This paper builds on previous work [17-19]; the work is extended here to consider the fully three-dimensional effect of the soil on a buried fluid-filled pipe. The pipe is

modelled as a thin cylindrical shell of linear homogeneous isotropic elastic material buried in an elastic medium of infinite extent. Considering the surrounding medium to exert effects on the pipe in all directions, expressions for the wavenumbers are derived for $n = 0$ axisymmetric motion; then the propagation wavespeed and wave attenuation of the $s = 1$ wave and $s = 2$ wave are analyzed. At the pipe/soil interface, two extreme cases can be considered, representing the coupling extremes, in order to investigate the shear coupling: the first is termed the "slip" condition, in which there is lubricated contact between the pipe and the surrounding soil, and no accompanying shear stress; the second is termed the "no slip" condition in which compact contact between the pipe and the surrounding soil is assumed and for which there is continuity of tangential displacement across the boundary. Here, the "slip" case is considered, for which low-frequency (when there is less than one half of a fluid wavelength across the pipe diameter), analytical expressions for the s=1 and s=2 wavenumbers can be derived, permitting insights to be gained into the physical mechanisms at play. These cases are then compared with the situation in which no shear wave is present in the surrounding medium, i.e. either when there is no surrounding medium or when the pipe is immersed in a fluid. In order to demonstrate the predicted behaviour, some example results for two typical soils are presented. To validate the theoretical predictions, additional example results are compared with experimental measurements made on a buried plastic pipe.

The paper is organized as follows: in section 2, the equations of motion for the pipe and surrounding soil are derived; in section 3, analytic solutions are derived, and their implications discussed; section 4 presents the example results; in section 5, additional example results are compared with experimental measurements; finally, in section 6, the conclusions are presented.

2. Equations of motion

2.1 Vibration of the pipe

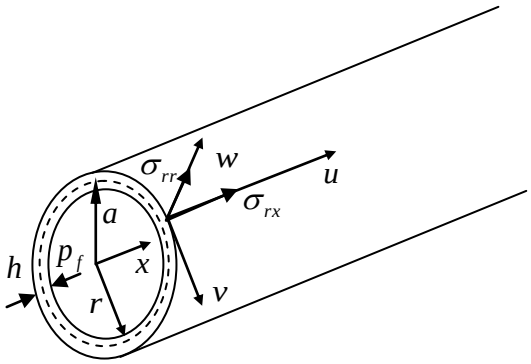

Figure. 1. The co-ordinate system for a buried fluid-filled pipe

The pipe equations for $n = 0$ axisymmetric wave motion are derived for a buried fluid-filled pipe. The surrounding soil is regarded as an infinite elastic medium which can sustain both compressional and shear waves. A semi-infinite cylindrical shell is shown in Fig. 1: the shell displacements are u, v and w in the axial (x), circumferential (θ), and radial (r) directions, respectively; a and h are the pipe radius and wall thickness respectively. The contained fluid imposes a pressure (p_f) on the pipe wall; the surrounding soil imposes both tangential and normal stresses. The following are simplified forms of Kennard's equations for a thin-walled shell [20], with shell bending neglected, and so are only valid below the ring frequency.

Equilibrium of forces in the axial direction gives

$$\rho_p \ddot{u} = \partial \sigma_x / \partial x + \sigma_{rx}(a)/h \tag{1}$$

Equilibrium of forces in the radial direction, assuming no circumferential variation, leads to

$$\left(p_f(a) + \sigma_{rr}(a)\right)(a/h) = \sigma_\theta + \rho_p a \ddot{w} \tag{2}$$

(note that the pressure and stresses are evaluated at $r = a$), where σ_x, σ_θ are circumferential and axial stresses in the shell, σ_{rx}, σ_{rr} are stresses in the external elastic medium; ρ_p is the density of the shell material; a and h are the radius and thickness of the shell wall respectively ($h << a$). Hooke's Law for the shell gives

$$\sigma_\theta = \frac{E_p}{1-\nu_p^2}\left(\frac{w}{a} + \nu\frac{\partial u}{\partial x}\right), \quad \sigma_x = \frac{E_p}{1-\nu_p^2}\left(\frac{\partial u}{\partial x} + \nu\frac{w}{a}\right) \tag{3, 4}$$

Where E_p and ν_p are the elastic modulus and Poisson's ratio for the pipe material respectively. Combining equations (1) and (4) gives

$$\rho_p \ddot{u} - \frac{E_p}{1-\nu_p^2}\left(\frac{\partial^2 u}{\partial x^2} + \frac{\nu}{a}\frac{\partial w}{\partial x}\right) - \frac{1}{h}\sigma_{rx}(a) = 0 \tag{5}$$

Equations (2) and (3) yield

$$\rho_p a\ddot{w} + \frac{E_p}{1-\nu_p^2}\left(\frac{w}{a} + \nu\frac{\partial u}{\partial x}\right) = \left(p_f(a) + \sigma_{rr}(a)\right)\frac{a}{h} \tag{6}$$

these are the two coupled shell equations for $n = 0$ motion.

Travelling wave solutions of the form

$$u = \sum_{s=1}^{2} U_s \mathrm{e}^{\mathrm{i}(\omega t - k_s x)}, \quad w = \sum_{s=1}^{2} W_s \mathrm{e}^{\mathrm{i}(\omega t - k_s x)} \tag{7, 8}$$

may be used to describe the pipe displacements, where ω is the angular frequency and k_s is the axial wavenumber for the s wave.

2.2 Vibration of the contained fluid

Assuming that the internal medium is a fluid, which cannot sustain shear, the internal pressure p_f can be described by a Bessel function of order zero [21].

$$p_f = \sum_{s=1}^{2} P_{fs} \mathrm{J}_0\left(k_{fs}^r r\right) \mathrm{e}^{\mathrm{i}(\omega t - k_s x)} \tag{9}$$

where the internal fluid radial wavenumber, k_{fs}^r, is related to the fluid wavenumber, k_f, by

$$\left(k_{fs}^r\right)^2 = k_f{}^2 - k_s{}^2 \tag{10}$$

2.3 Vibration of the surrounding soil

The displacement vector, $\mathbf{u}(x, \theta, r, t)$, of a point in the surrounding medium satisfies the equation of motion [22] (eq. A.3)

$$\left(\lambda_m + \mu_m\right)\nabla(\Delta) + \mu_m \nabla^2 \mathbf{u} = \rho_m \frac{\partial^2 \mathbf{u}}{\partial t^2} \tag{11}$$

Where λ_m, μ_m are the Lame coefficients; ρ_m is the density of the medium; ∇ is Hamilton differential operator; Δ is the dilatation which in cylindrical coordinates is given by

$$\Delta = \frac{1}{r}\frac{\partial(r u_r)}{\partial r} + \frac{1}{r}\frac{\partial u_\theta}{\partial \theta} + \frac{\partial u_x}{\partial x} \tag{12}$$

where u_r, u_θ and u_x are the displacements of the soil in the r, θ and x directions, respectively.

The components of the rotation about the three orthogonal directions are given by [22] (eq. 3.39)

$$\left.\begin{aligned}\varpi_r &= \frac{1}{2}\left(\frac{1}{r}\frac{\partial u_x}{\partial \theta} - \frac{\partial u_\theta}{\partial x}\right)\\ \varpi_\theta &= \frac{1}{2}\left(\frac{\partial u_r}{\partial x} - \frac{\partial u_x}{\partial r}\right)\\ \varpi_x &= \frac{1}{2r}\left(\frac{\partial (r u_\theta)}{\partial r} - \frac{\partial u_r}{\partial \theta}\right)\end{aligned}\right\} \qquad (13a, b, c)$$

According to Hooke's Law, the relationship between the stresses and the strains are given by [22] (eq. 3.41)

$$\left.\begin{aligned}\sigma_{rr} &= \lambda_m \Delta + 2\mu_m \frac{\partial u_r}{\partial r}\\ \sigma_{r\theta} &= \mu_m\left(\frac{1}{r}\frac{\partial u_r}{\partial \theta} + r\frac{\partial}{\partial r}\left(\frac{u_\theta}{r}\right)\right)\\ \sigma_{rx} &= \mu_m\left(\frac{\partial u_r}{\partial x} + \frac{\partial u_x}{\partial r}\right)\end{aligned}\right\} \qquad (14a, b, c)$$

For axisymmetric motion, the displacement u_θ vanishes ($u_\theta = 0$), as do variations with respect to θ ($\partial / \partial \theta = 0$). Thus, equations (12) and (13) become

$$\Delta = \frac{1}{r}\frac{\partial (r u_r)}{\partial r} + \frac{\partial u_x}{\partial x}, \quad \varpi_\theta = \frac{1}{2}\left(\frac{\partial u_r}{\partial x} - \frac{\partial u_x}{\partial r}\right) \qquad (15, 16)$$

Similar to the pipe displacements, travelling wave solutions for the surrounding medium may be assumed of the form

$$u_r = W_m \mathrm{e}^{\mathrm{i}(\omega t - k_s x)}, \quad u_x = U_m \mathrm{e}^{\mathrm{i}(\omega t - k_s x)} \qquad (17, 18)$$

where both W_m and U_m are functions of radius, r. Combining equations (11), (15)-(18) gives the equations of motion in the surrounding medium as [22] (eqs. 3.45, 3.46)

$$\frac{\partial^2 \Delta}{\partial r^2} + \frac{1}{r}\frac{\partial \Delta}{\partial r} + \left(k_{ds}^r\right)^2 \Delta = 0 \qquad (19)$$

$$\frac{\partial^2 \varpi_\theta}{\partial r^2}+\frac{1}{r}\frac{\partial \varpi_\theta}{\partial r}-\frac{\varpi_\theta}{r^2}+\left(k_{rs}^r\right)^2\varpi_\theta=0 \tag{20}$$

where the surrounding medium compressional and shear radial wavenumbers, k_{ds}^r and k_{rs}^r respectively are given by $\left(k_{ds}^r\right)^2=k_d{}^2-k_s{}^2$, $\left(k_{rs}^r\right)^2=k_r{}^2-k_s{}^2$. k_d, k_r are the compressional (dilatational) and shear (rotational) wavenumbers in the surrounding medium, given by $k_d{}^2=\rho_m\omega^2/\left(\lambda_m+2\mu_m\right)$ and $k_r{}^2=\rho_m\omega^2/\mu_m$, respectively.

Equations (19), (20) are Bessel's equations, so solutions of the above two equations for an external cylindrical space are

$$\Delta=G\mathrm{H}_0\left(k_{ds}^r r\right),\quad \varpi_\theta=H\mathrm{H}_1\left(k_{rs}^r r\right) \tag{21, 22}$$

where G and H are function of x and t, but are independent of r. $\mathrm{H}_0(\ )$, $\mathrm{H}_1(\ )$ are Hankel functions of the second kind which describe outgoing waves.

Substituting for u_r and u_x from equations (17), (18) into (19), (20), give

$$\Delta=\left(\frac{\partial W_m}{\partial r}+\frac{W_m}{r}-\mathrm{i}k_s U_m\right)\exp\left[\mathrm{i}(\omega t-k_s x)\right] \tag{23}$$

$$\varpi_\theta=\frac{1}{2}\left(-\mathrm{i}k_s W_m-\frac{\partial U_m}{\partial r}\right)\exp\left[\mathrm{i}(\omega t-k_s x)\right] \tag{24}$$

In order to satisfy equations (21)-(24), U_m and W_m must have the form [22]

$$W_m=A\frac{\partial}{\partial r}\left[\mathrm{H}_0\left(k_{ds}^r r\right)\right]-Ck_x\mathrm{H}_1\left(k_{rs}^r r\right) \tag{25}$$

$$U_m=-\mathrm{i}Ak_x\mathrm{H}_0\left(k_{ds}^r r\right)+\frac{\mathrm{i}C}{r}\frac{\partial}{\partial r}\left[r\mathrm{H}_1\left(k_{rs}^r r\right)\right] \tag{26}$$

where A and C are constants.

From equations (14), (25) and (26), the stresses in the surrounding soil can be expressed in terms of A and C as

$$\sigma_{rr} = A\left[2\mu_m\left(k_{ds}^r\right)^2 \mathrm{H}_0''\left(k_{ds}^r\right) - \lambda_m k_d^2 \mathrm{H}_0\left(k_{ds}^r\right)\right] - 2C\mu_m k_s k_{rs}^r \mathrm{H}_1\left(k_{rs}^r r\right) \tag{27}$$

$$\sigma_{rx} = i\mu_m\left[-2Ak_s k_{ds}^r \mathrm{H}_0'\left(k_{ds}^r\right) + C\left(2k_s^2 - k_r^2\right)\mathrm{H}_1\left(k_{rs}^r r\right)\right] \tag{28}$$

$\sigma_{rx} = i\mu[\ ]$

where $\mathrm{H}_n'(\ ) = \dfrac{\partial}{\partial r}\mathrm{H}_n(\ ),\ \ \mathrm{H}_n''(\ ) = \dfrac{\partial^2}{\partial r^2}\mathrm{H}_n(\ ).$

2.4 Fully coupled equations

The coefficient P_{fs} in equation (9) and the coefficients A, C in equations (25)-(28) may be determined from the conditions at the pipe/internal fluid and pipe/soil interfaces respectively.

2.4.1 Pipe/internal fluid interface

For the fluid, at the boundary $r = a$, each of the s=1,2 pressure waves in the contained fluid must have a radial displacement at the shell boundary r=a which is equal to the shell displacement. Equating the radial velocity of the fluid at the shell wall to the radial velocity of the shell wall gives

$$P_{fs} = \omega^2 \rho_f W_s \Big/ \left(k_{fs}^r \mathrm{J}_0'\left(k_{fs}^r a\right)\right) \tag{29}$$

Combining equations (9), (25) and (31) gives

$$p_{f(a)} = \omega^2 \rho_f \left[A\frac{\partial}{\partial r}\left[\mathrm{H}_0\left(k_{ds}^r a\right)\right] - Ck_s \mathrm{H}_1\left(k_{rs}^r a\right)\right]\frac{\mathrm{J}_0\left(k_{fs}^r a\right)}{k_{fs}^r \mathrm{J}_0'\left(k_{fs}^r a\right)} \tag{30}$$

2.4.2 Pipe/soil interface

For the pipe/soil interface, we consider one extreme case, termed the “slip” case. Here the pipe and soil are considered to be in lubricated contact so that the shear

stress vanishes along the pipe surface.

Equation (28) thus becomes

$$-2Ak_s k_{ds}^r \mathrm{H}_0'\left(k_{ds}^r a\right)+C\left[2k_s{}^2-k_r{}^2\right]\mathrm{H}_1\left(k_{rs}^r a\right)=0 \tag{31}$$

Furthermore, the displacements of the soil in the radial direction must match that of the shell, i.e.,

$$W_m = W_s \tag{32}$$

Substituting equations (25), (27), (28), (30), (31) and (32), into equations (5) and (6), eliminating the constants *A* and *C*, and rearranging results in the following dispersion equation for the *s* waves.

$$\left[1-k_L{}^2a^2+v_p^2\frac{k_s{}^2}{k_L{}^2-k_s{}^2}\right]=\frac{1-v_p^2}{E_p h}\left\{\begin{array}{l} B_f a k_f^2 a^2\dfrac{\mathrm{J}_0\left(k_{fs}^r a\right)}{k_{fs}^r a\mathrm{J}_0'\left(k_{fs}^r a\right)}+\lambda_m a\dfrac{k_d{}^2a^2}{k_{ds}^r a}\left[2\dfrac{k_s{}^2}{k_r{}^2}-1\right]\dfrac{\mathrm{H}_0\left(k_{ds}^r a\right)}{\mathrm{H}_0'\left(k_{ds}^r a\right)} \\ -2\mu_m a k_{ds}^r a\left[2\dfrac{k_s{}^2}{k_r{}^2}-1\right]\dfrac{\mathrm{H}_0''\left(k_{ds}^r a\right)}{\mathrm{H}_0'\left(k_{ds}^r a\right)}+4\mu_m a\dfrac{k_s{}^2}{k_r{}^2}k_{rs}^r a\dfrac{\mathrm{H}_1'\left(k_{rs}^r a\right)}{\mathrm{H}_1\left(k_{rs}^r a\right)} \end{array}\right\} \tag{33}$$

where k_L is the wavenumber of a compressional wave in the empty pipe shell wall , given by $k_L{}^2=\omega^2\rho_p(1-v_p^2)/E_p$ and B_f is the bulk modulus of the internal fluid. This is the wavenumber, or dispersion, equation.

3. Analytic solutions

Equation (33) is, in general, not amenable to analytic solution. However, some cases may be looked at in more detail. Since acoustic energy in buried water pipes generated by a leak propagates at relatively low frequencies [8], the behaviour of these waves at low frequencies is the focus of attention here. By using low-frequency approximations, when there is less than half a fluid wavelength across the pipe

diameter, some relatively simple wavenumber solutions may be found, enabling physical interpretations to be offered.

Here, the small argument approximations for the Bessel functions $\frac{\mathrm{J}_0\left(k_{fs}^r a\right)}{\mathrm{J}_0'\left(k_{fs}^r a\right)} \approx -\frac{2}{k_{fs}^r a}$, as given in the Appendix, may be used [23]. Equation (33) then simplifies to

$$\left[1-{k_L}^2 a^2+\nu_p^2\frac{{k_s}^2}{{k_L}^2-{k_s}^2}\right]=\frac{1-\nu_p^2}{E_p h}\left\{\begin{array}{l} 2B_f a\frac{{k_f}^2}{{k_f}^2-{k_s}^2}+i\omega a^2\frac{\lambda_m}{\lambda_m+2\mu_m}\left[1-2\frac{k_s^2}{k_r^2}\right]z_{rad} \\ -2\mu_m a\left[1-2\frac{{k_s}^2}{{k_r}^2}\right]k_{ds}^r a\frac{\mathrm{H}_0''\left(k_{ds}^r a\right)}{\mathrm{H}_0'\left(k_{ds}^r a\right)}-4\mu_m a\frac{{k_s}^2}{{k_r}^2}k_{rs}^r a\frac{\mathrm{H}_1'\left(k_{rs}^r a\right)}{\mathrm{H}_1\left(k_{rs}^r a\right)} \end{array}\right\} \tag{34}$$

where $z_{rad}=-i\rho_m c_d\frac{k_d}{k_{ds}^r}\frac{H_0\left(k_{ds}^r a\right)}{H_0'\left(k_{ds}^r a\right)}$ is the radiation impedance of the compressional wave in the surrounding medium, in the absence of shear [17]. Equation (34) allows the two s wavenumbers to be determined, $s=1,2$, corresponding to a fluid-dominated wave and an axial shell-dominated wave, respectively.

3.1 Shear modulus μ_m =0

When the surrounding medium is a fluid, there will be no shear. In this case, the shear modulus $\mu_m=0$, and consequently the shear wavenumber $k_r\to\infty$. Equation (34) then becomes

$$1-{k_L}^2 a^2+\nu_p^2\frac{{k_s}^2}{{k_L}^2-{k_s}^2}=-\frac{2B_f a\left(1-\nu_p^2\right)}{E_p h}\frac{{k_f}^2}{{k_f}^2-{k_s}^2}-\frac{B_m a\left(1-\nu_p^2\right)}{E_p h}\frac{{k_d}^2 a^2\mathrm{H}_0\left(k_{ds}^r a\right)}{k_{ds}^r a\mathrm{H}_0'\left(k_{ds}^r a\right)} \tag{35}$$

where B_m is the bulk modulus of the surrounding fluid.

This is in agreement with the solution presented in [17] (equation 19), setting the shear modulus to zero.

3.2 The s=1 wave

The $s=1$ wavenumber (the predominantly fluid-borne wave) is found by assuming that k_1 is much larger than the plate compressional wavenumber k_L: i.e., the wavespeed of the $s=1$ wave is much slower than the plate compressional wavespeed. Setting $k_1^2 >> k_L^2$ in equation (34) results in the following expression for the $s=1$ wave.

$$k_1^2 = k_f^2 \left\{ 1 + \frac{2B_f / a}{E_p h / a^2 - \omega^2 \rho_p h + i\omega \frac{\lambda_m}{\lambda_m + 2\mu_m} \left[1 - 2\frac{k_1^2}{k_r^2} \right] z_{rad1} - 2\frac{\mu_m}{a} \left[1 - 2\frac{k_1^2}{k_r^2} \right] k_{d1}^r a \frac{\mathrm{H}_0''\left(k_{d1}^r a\right)}{\mathrm{H}_0'\left(k_{d1}^r a\right)} - 4\frac{\mu_m}{a}\frac{k_1^2}{k_r^2} k_{r1}^r a \frac{\mathrm{H}_1}{\mathrm{H}_1} \right.$$

(36)

Expressing k_1 in this form allows most of the individual terms to be readily identified: the stiffness components of the contained fluid ($2B_f / a$) and the pipe wall ($E_p h / a^2$); a pipe wall mass component ($\omega^2 \rho_p h$); and the *s*=1 compressional wave impedance term $i\omega \frac{\lambda_m}{\lambda_m + 2\mu_m} \left[1 - 2\frac{k_1^2}{k_r^2} \right] z_{rad1}$. The remaining two terms, $2\frac{\mu_m}{a} \left[1 - 2\frac{k_1^2}{k_r^2} \right] k_{d1}^r a \frac{\mathrm{H}_0''\left(k_{d1}^r a\right)}{\mathrm{H}_0'\left(k_{d1}^r a\right)}$ and $4\frac{\mu_m}{a}\frac{k_1^2}{k_r^2} k_{r1}^r a \frac{\mathrm{H}_1'\left(k_{r1}^r a\right)}{\mathrm{H}_1\left(k_{r1}^r a\right)}$, are radiation terms associated with the compressional and shear waves in the surrounding medium when shear is present.

At, in general, slightly lower frequencies, when the radial wavenumbers in the

surrounding medium are small compared with a pipe radius ($k_{d1}^r a << 1, k_{r1}^r a << 1$), the small argument approximations for the Hankel function ratios, $\frac{\mathrm{H}_0''\left(k_{d1}^r a\right)}{\mathrm{H}_0'\left(k_{d1}^r a\right)}$ and $\frac{\mathrm{H}_1'\left(k_{r1}^r a\right)}{\mathrm{H}_1\left(k_{r1}^r a\right)}$ given in the Appendix, may be used. Equation (36) then simplifies to

$$k_1^2 = k_f^2\left(1+\frac{2B_f/a}{E_p h/a^2 - \omega^2\rho_p h + i\omega\frac{\lambda_m}{\lambda_m+2\mu_m}\left(1-2\frac{k_1^2}{k_r^2}\right)z_{rad1}+2\mu_m/a}\right) \quad (37)$$

Here, the radiation terms, dependent on shear, become a single shear stiffness term, $2\mu_m$/a.

At very low frequencies, the ω^2 term and the compressional wave impedance, z_{rad}, both tend to zero, so equation (37) becomes

$$k_1^2 = k_f^2\left(1+\frac{2B_f/a}{E_p h/a^2 + 2\mu_m/a}\right) \quad (38)$$

This is also in accordance with the expression given in [16] for low frequency tube waves.

For the case of no surrounding medium, equation (37) reduces to

$$k_1^2 = k_f^2\left(1+\frac{2B_f/a}{E_p h/a^2 - \omega^2\rho_p h}\right) \quad (39)$$

agreeing with earlier work by Pinnington and Briscoe [9]. Comparing equations (36), (37) and (38) with equation (39), it can be seen that, at very low frequencies, the effect of the surrounding soil is to add stiffness; at slightly higher frequencies when

the compressional wave impedance term starts to contribute, there is an added mass and radiation damping effect, similar to that described in [17], largely controlled by the compressional wave. At slightly higher frequencies still, the effect of shear is more complex with both real and imaginary terms contributing. The nature of this shear contribution will be examined more fully in section 4 where example results are presented.

3.3 The s=2 wave

For the $s=2$ wave, setting $k_2^{\,2} << k_f^{\,2}$ in equation (34), k_2 becomes

$$k_2^2 = k_L^2\left\{1+\frac{\nu_p^2}{1-\nu_p^2}\frac{E_p h/a^2}{E_p h/a^2-\omega^2\rho_p h+2B_f/a+i\omega\dfrac{\lambda_m}{\lambda_m+2\mu_m}\left[1-2\dfrac{k_2^2}{k_r^2}\right]z_{rad2}-2\dfrac{\mu_m}{a}\left[1-2\dfrac{k_2^{\,2}}{k_r^{\,2}}\right]k_{d2}^r a\dfrac{\mathrm{H}_0''\left(k_{d2}^r a\right)}{\mathrm{H}_0'\left(k_{d2}^r a\right)}-4\dfrac{\mu_m}{a}\dfrac{k_2^{\,2}}{k_r^{\,2}}k_{r2}^r a\dfrac{\mathrm{H}_1}{\mathrm{H}_1}\right.\right.$$

(40)

Again the individual terms can be readily identified with the radiation terms here being associated with the s=2 wave. At, in general, slightly lower frequencies, the small argument approximations for the Hankel function ratios (see Appendix) may again be used giving

$$k_2^2 = k_L^2\left(1+\frac{\nu_p^2}{1-\nu_p^2}\frac{E_p h/a^2}{E_p h/a^2-\omega^2\rho_p h+2B_f/a+i\omega\dfrac{\lambda_m}{\lambda_m+2\mu_m}\left(1-2\dfrac{k_2^2}{k_r^2}\right)z_{rad2}+2\mu_m/a}\right)$$

(41)

Again the shear radiation terms become a single shear stiffness.

At very low frequencies equation (41) becomes

$$k_2^2 = k_L^2\left(1+\frac{\nu_p^2}{1-\nu_p^2}\frac{E_p h/a^2}{E_p h/a^2+2B_f/a+2\mu_m/a}\right) \qquad (42)$$

For the case of no surrounding medium, equation (41) reduces to

$$k_2^2 = k_L^2\left(1+\frac{\nu_p^2}{1-\nu_p^2}\frac{E_p h/a^2}{E_p h/a^2-\omega^2\rho_p h+2B_f/a}\right) \tag{43}$$

again agreeing with earlier work by Pinnington and Briscoe [9]. As for the s=1 wave, it can be seen that, at very low frequencies, the effect of shear is to add stiffness. At higher frequencies, as before, mass and radiation damping are added via the compressional wave impedance, largely controlled by the compressional wave. Again at slightly higher frequencies, the effect of shear becomes complex.

4. Example results

In this section example results are presented for typical PVC water pipe surrounded by a medium which can sustain both compressional and shear waves. Complex wavenumbers for both the s=1 and s=2 waves are plotted as a function of frequency, where the real part gives the wave propagation speed, and the imaginary part gives the wave attenuation. Loss within the pipe wall is included, and is achieved by means of a complex modulus of elasticity. All the results are non-dimensionalized by the pipe radius, a, and plotted against the non-dimensional free field fluid wavenumber $k_f a$. Two soils, denoted A and B, have been chosen to represent typical sandy (A) and clay or chalky (B) soils respectively [24]. Soil B also provides continuity with the previous work carried out in [17]. The various pipe and media properties are shown in Tables 1 and 2.

Table 1 Pipe properties

Properties	Pipe
Thickness/radius ratio	0.125
Elastic modulus (N/m^2)	5.0×10^9

Density (kg/m^3)	2000
Poisson's ratio	0.4
Material loss factor	0.065
Plate compressional wavespeed (m/s)	1725

Table 2 Soil and fluid properties

Properties	Soil *A*	Soil *B*	Fluid
Bulk modulus (N/m^2)	5.3x10^7	4.5×10^9	2.25×10^9
Shear modulus (N/m^2)	2.0x10^7	1.8×10^8	—
Density (kg/m^3)	2000	2000	1000
Compressional wavespeed (m/s)	200	1540	1500
Shear wavespeed (m/s)	100	300	—

Here it should be noted that, when computing the *s* wavenumbers from equations (36) and (39), the radiation impedance terms, $i\omega a^2 \frac{\lambda_m}{\lambda_m + 2\mu_m}\left[1 - 2\frac{k_s^2}{k_r^2}\right] z_{rad}$, $2\frac{\mu_m}{a}\left[1 - 2\frac{k_s^{\ 2}}{k_r^{\ 2}}\right] k_{ds}^r a \frac{\mathrm{H}_0''\left(k_{ds}^r a\right)}{\mathrm{H}_0'\left(k_{ds}^r a\right)}$ and $4\frac{\mu_m}{a}\frac{k_s^{\ 2}}{k_r^{\ 2}} k_{rs}^r a \frac{\mathrm{H}_1'\left(k_{rs}^r a\right)}{\mathrm{H}_1\left(k_{rs}^r a\right)}$ are a function of the *s* wavenumber so the calculation must be performed recursively. Furthermore, considering the arguments of the Hankel functions, which are derived from square root, it is important to choose the sign of the root correctly. This is a straightforward matter when the argument is purely real or purely imaginary as the sign is chosen such that the radial component of the wave in the surrounding medium either propagates outwards from the shell (real argument, homogeneous partial wave) or decays away from it (imaginary argument, inhomogeneous partial wave). When the argument is complex, the sign of the root is chosen according to whether the real or

imaginary part of the argument is larger [25]. If the real part is larger, the partial wave can be considered homogeneous and must propagate away from the shell, so the positive square root is chosen; if the imaginary part is larger, the partial wave can be considered inhomogeneous and must decay away from the shell, so the negative square root is chosen.

4.1 The s=1 wave

Figure 2(a) shows the real part of the s=1 wavenumber for soil *A*. It can be seen that, as expected, without the surrounding medium, the effect of the pipe wall is to substantially increase the real part of the *s*=1 wavenumber from the freefield value, k_f, (also shown in the figure). With a surrounding medium, but neglecting the effects of shear (treating the medium as a fluid as in [17]), the real part of the wavenumber increases yet further indicating that the effect of the 'fluid' is one of mass loading. Once the full effects of shear are included, the real part of the wavenumber falls below the case of no surrounding medium showing that, the effect of shear is to add stiffness. Adopting the low-frequency approximations for the shear controlled radiation terms has the advantage of making the effect of shear explicit and can be seen to be valid for all the frequencies shown. However, as found previously [17], the additional effect of the surrounding medium is small compared with the effect of the shell wall. This is seen even more clearly in Figure 2(b) which presents the same results in terms of the wavespeed of the s=1 wave (inversely proportional to wavenumber), normalized by the free field wavespeed. In this figure, an additional curve has been plotted, derived from a simplified form of equation (37) in which the compressional radiation impedance term has been neglected, giving

$$k_1^2 = k_f^2\left(1+\frac{2B_f/a}{E_p h/a^2-\omega^2\rho_p h+2\mu_m/a}\right)$$

(44)

The wavespeed varies only between 34% and 36% of the freefield wavespeed regardless of the conditions external to the pipe. Furthermore, the predicted wavespeed using the simplified formulation differs by less than 0.5% of the free field value compared with the complete formulation including the full effects of shear.

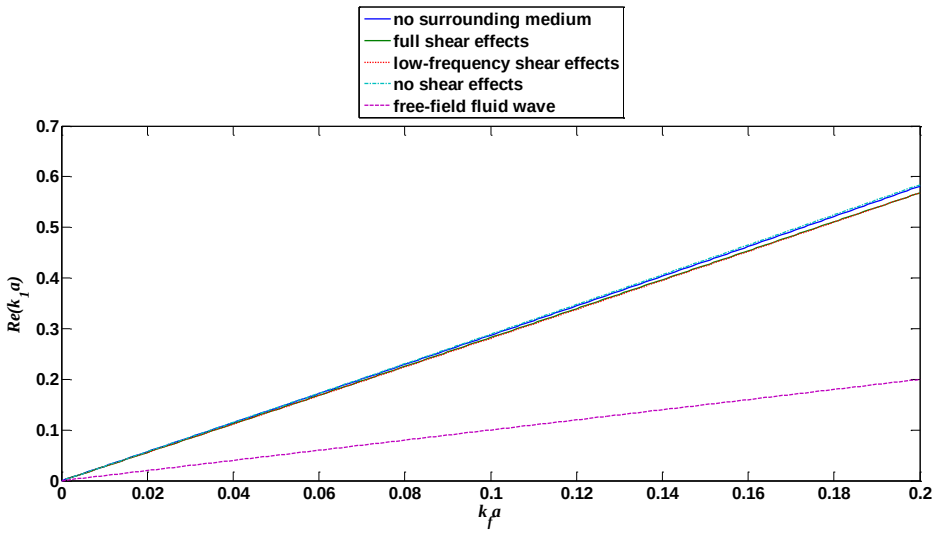

(a)

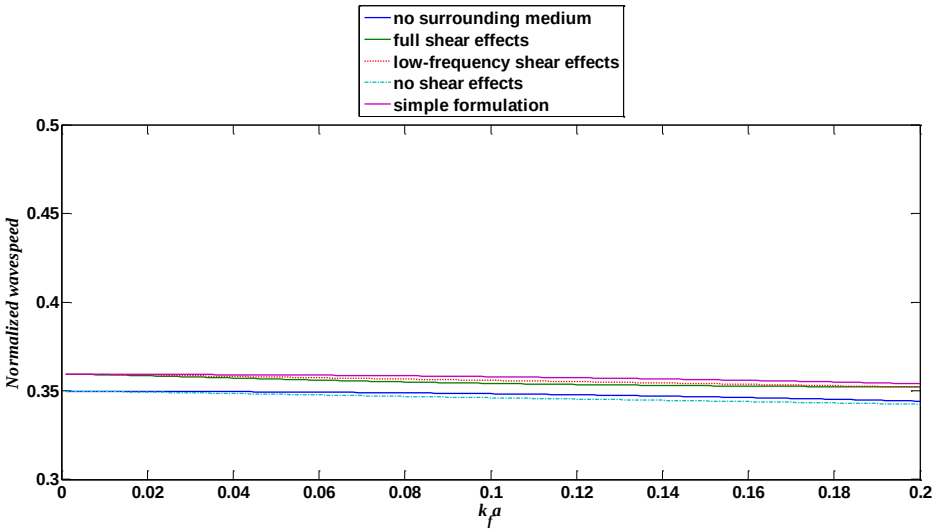

(b)

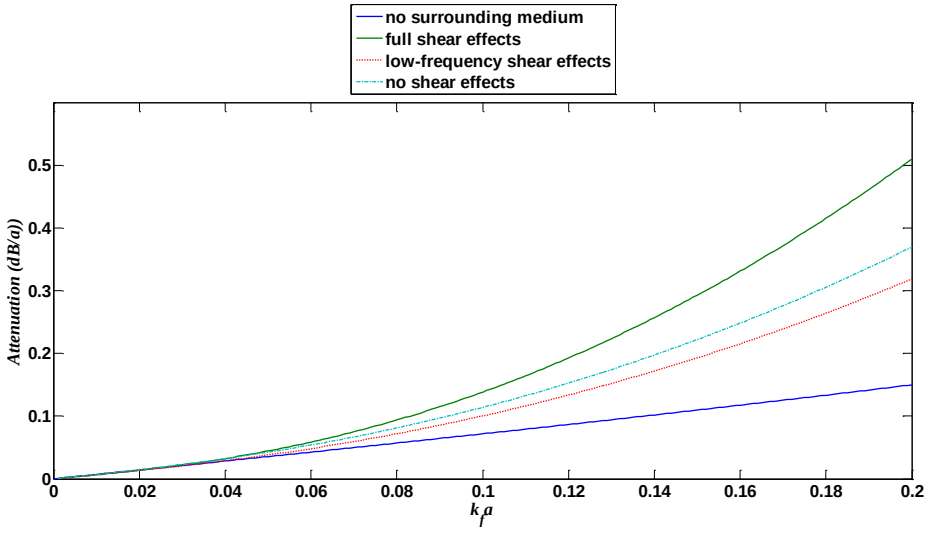

(c)

Figure 2

Wavenumbers & wavespeed for s=1 wave, soil *A*

(a) Real part; (b) Wavespeed; (c) Imaginary part

Figure 2(c) shows the loss in dB per unit propagation distance (measured in pipe radii). This is related to the imaginary part of the wavenumber by

$$\text{Loss (dB/unit distance } a) = 20\,\frac{\mathrm{Im}\{ka\}}{\ln(10)} \tag{45}$$

The *s*=1 wavenumbers in Figure 2(a) all correspond to wavespeeds of around 500m/s suggesting that both compressional (200m/s) and shear (100m/s) waves will radiate into the surrounding medium. That radiation into the surrounding medium occurs is confirmed by the finding that the *s*=1 wave attenuation increases significantly in its presence. At the lower end of the frequency range considered ($k_f a<0.05$), the attenuation can be seen to be dominated by losses within the pipe wall as there is little increase in the presence of the any surrounding medium. At higher frequencies, radiation as both compressional waves and shear waves contributes to the

attenuation. Here, adopting the low-frequency approximations for the Hankel function ratios results in an underestimation of the overall attenuation, in fact reducing it below the 'no shear' case (fluid surround); this is due to the term $\frac{\lambda_m}{\lambda_m + 2\mu_m}\left[1 - 2\frac{k_1^2}{k_r^2}\right]$ reducing the effect of the compressional radiation impedance, z_{rad1}.

Figure 3(a) shows the real part of the s=1 wavenumber for soil *B*. Here the same trends are observed as for soil *A* but, in this case, more pronounced: with no shear effects in the surrounding medium an added mass effect is seen; including the effects of shear adds stiffness. The effects are greater for soil *B* as both the shear modulus and the bulk modulus are greater than for soil *A*, whilst the density is unchanged. Again, adopting the low-frequency approximations for the Hankel function ratios is valid throughout the frequency range.

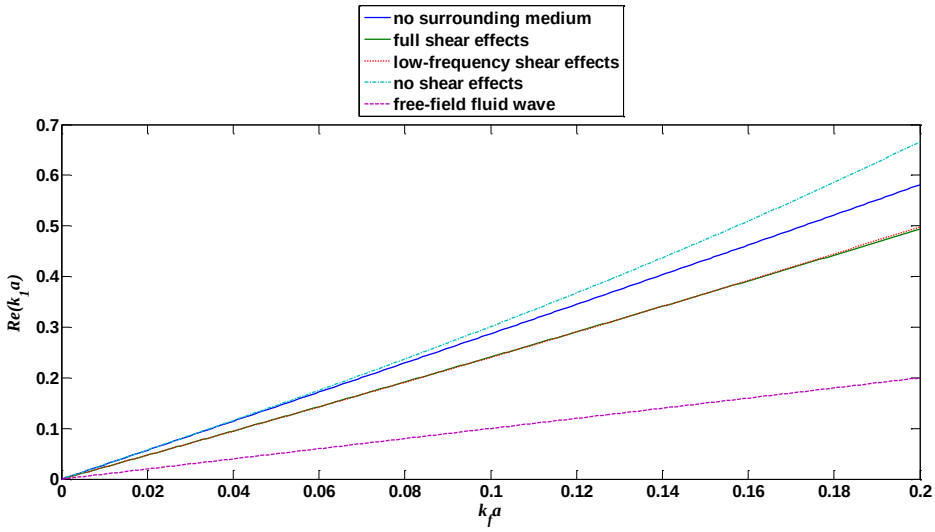

(a)

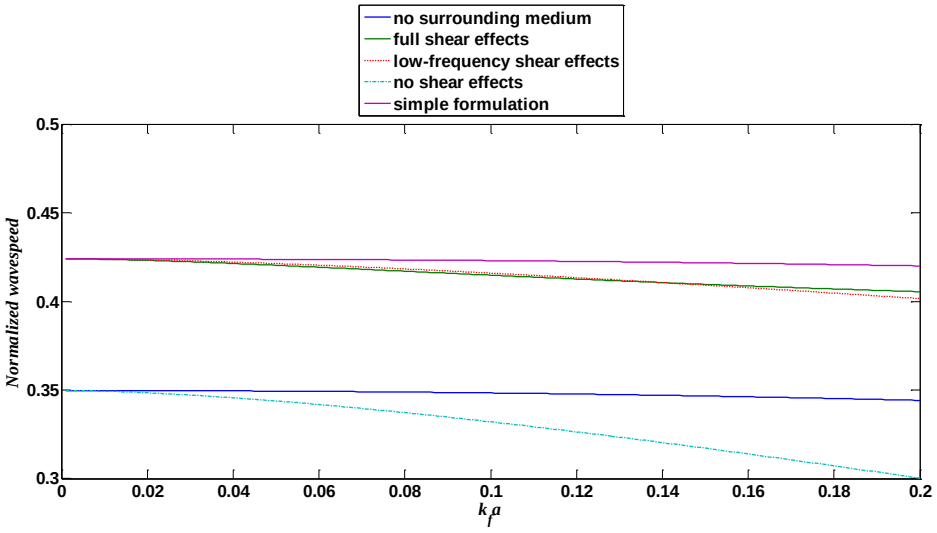

(b)

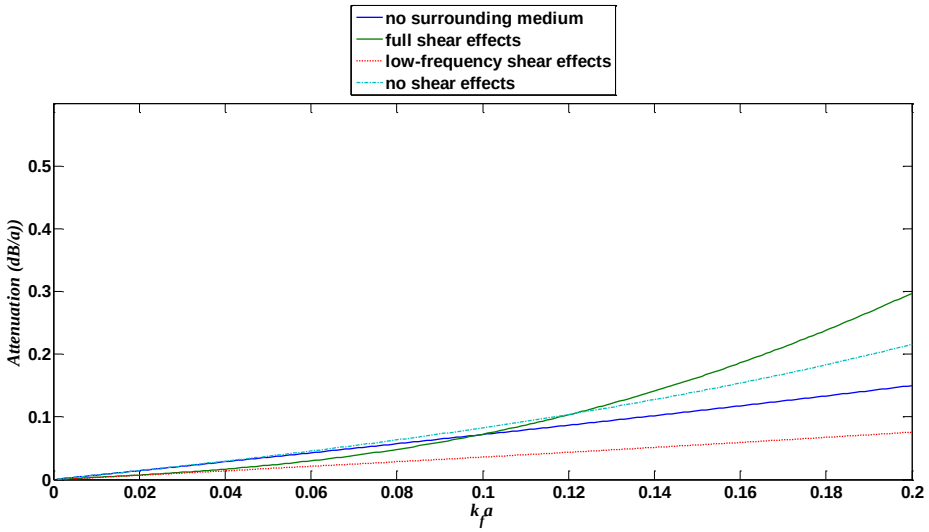

(c)

Figure 3

Wavenumbers and wavespeed for *s*=1 wave, soil *B*

(a) Real part; (b) Wavespeed; (c) Imaginary part

Figure 3(b) shows the normalized wavespeed. Compared with soil *A*, there is a greater variation in the wavespeed compared with the free-field value (30%-43%) but even here the effect of the pipe wall compliance dominates. Again the difference

between using the simplified formulation and the formulation including the full effects of shear is small (less than 1.5% of the free field value)

Figure 3(c) shows the loss in dB per unit propagation distance. Here, apparently surprising behaviour is observed. The presence of a surrounding medium without the effects of shear increases the attenuation. Here the s=1 wave would not be expected to radiate due to the fast speed of the compressional wave in soil *B*. Furthermore, including the effects of shear results in a decrease in attenuation at very low frequencies ($0<k_f a<0.1$), not only compared with the no shear case but also compared with the case of no surrounding medium. Additional checks revealed that the losses seen here are not related to radiation but to the losses within the pipe wall itself, the differences between the different cases being a result of changes in the wavespeed of the s=1 wave and the effects of a complex elastic modulus in equation (36). The s=1 wave would be expected to radiate as a shear wave and, when the results including the full effects of shear and those using the low-frequency Hankel function approximations are compared, it can be seen that it indeed does; particularly at higher frequencies ($0.05<k_f a<0.2$), using these approximations results in a significant underestimate of the attenuation.

4.2 The s=2 wave

Figure 4(a) shows the real part of the s=2 wavenumber for soil *A*. There is no discernible difference between the 'no surrounding medium' case and the other cases for which a surrounding medium is present. This is as expected given the stiffness of the contained fluid is large compared with both the pipe wall stiffness and the shear stiffness of the surrounding medium. Examination of Figure 4(b) depicting the attenuation shows that, unless the full shear-controlled radiation terms are included, the loss is unaffected by the surrounding medium. However, the s=2 wave would be

expected to radiate, both as a shear wave and a compressional wave and, once the full shear terms are included, this can be seen.

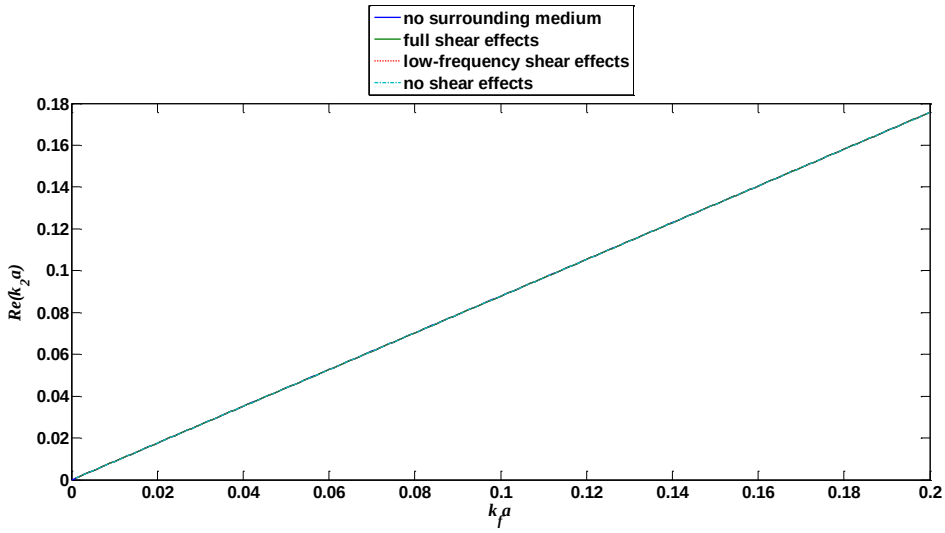

(a)

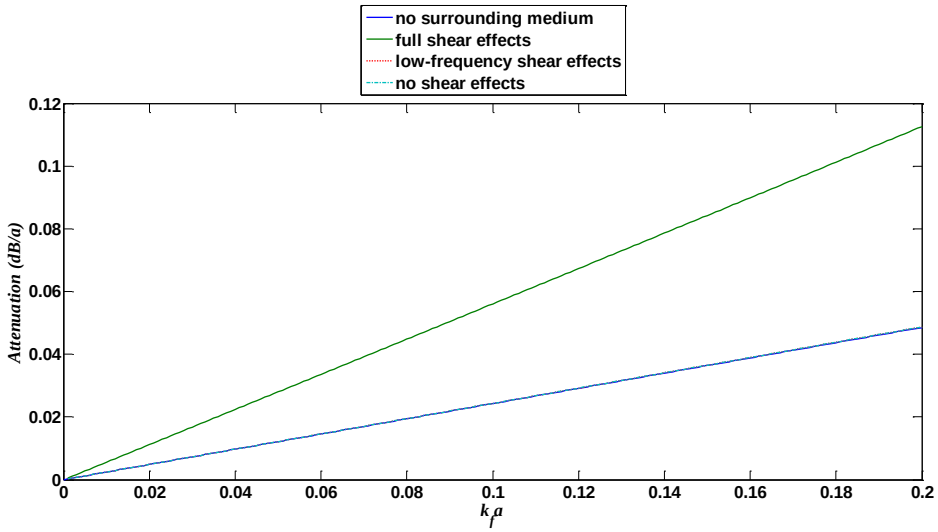

(b)

Figure 4

Wavenumbers for s=2 wave, soil *A*

(a) Real part; (b) Imaginary part

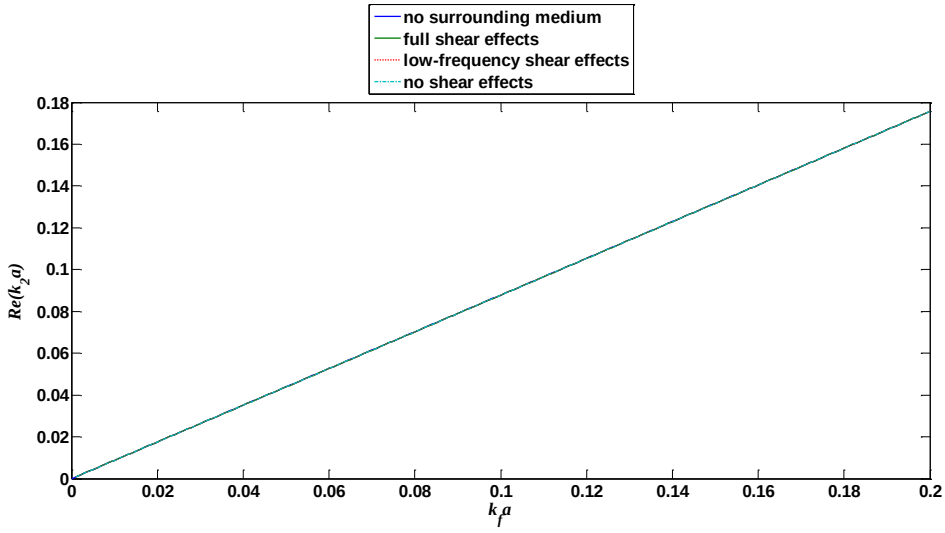

(a)

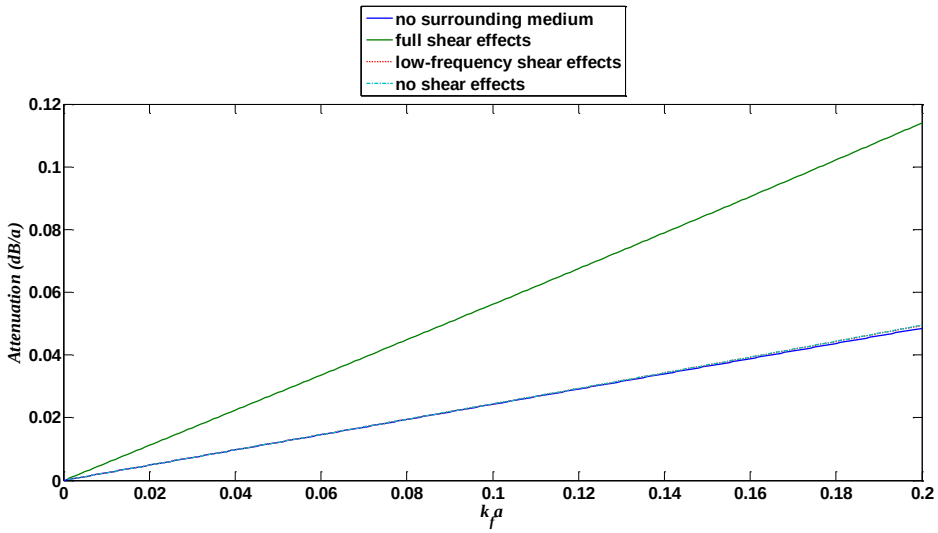

(b)

Figure 5

Wavenumbers for s=2 wave, soil *B*

(a) Real part; (b) Imaginary part

Figures 5(a,b) depict the results for soil *B*. Again the real part of the wavenumber is unaffected by the presence of the soil and, again, increased attenuation due to radiation is observed only once the full shear terms are included.

5. Experimental measurements

4.1 Background

Wavenumber measurements of the axisymmetric, fluid-dominated (n=0, s=1) wave in both *in vacuo* and buried fluid-filled plastic pipes have been made and reported on previously [18]. For the *in vacuo* pipe, the measurements were found to agree well with the theory (that given in equation (39) in the present paper). For the buried pipe, it was found that the wavenumber decreased relative to the *in vacuo* case, suggesting that the effect of the surrounding medium was to add stiffness. However, at the time, the buried pipe theoretical model available with which to make comparisons was that given in [17]. In this model, the effects of shear were not properly accounted for: the soil was effectively treated as a fluid supporting two different waves, each of which exerted normal pressure on the pipe wall. Thus, the model predicted the soil to exert a mass-loading effect, causing the s=1 wavenumber to increase, rather than decrease. The cause of the stiffening effect seen in the experiments was, at the time, attributed to a consequence of the low temperature of the soil (the measurements were made in winter): the increase in wavespeed was thought to be due to an increase in stiffness in the pipe wall. The elastic properties of MDPE (the pipe wall material) vary with temperature, the temperature in the ground being only a few degrees centigrade at the time of making the measurements, compared with around 20 degrees in the laboratory.

4.2 Experimental setup and procedure

Here, the experimental results are again presented, in the light of the theory described in the current paper. As stated previously, the s=1 wave is usually the main carrier of energy therefore of most interest; furthermore, the wavspeed of the s=2 wave is largely unaffected by either the contained fluid or the surrounding medium.

The details of the experimental setup and analysis can be found in [18] and are not reproduced in detail here. However, the key features are highlighted. The test rig comprised a 34m length, 180 mm OD, MDPE pipe buried at a depth of approximately 1m in loose, sandy soil. Loose, sandy soil is the ideal burial material for validating the "slip" boundary condition as the sand and the pipe are not likely to adhere very well, resulting in a very low shear stress at the pipe/sand boundary. The pipe was instrumented with a number of hydrophones along its length. The pipe was excited with a modified moving-coil underwater loudspeaker mounted in a flange at one end of the pipe. The loudspeaker was excited with a stepped sine input from 30 Hz to 1 kHz at 1 Hz intervals. Signals from a pair of hydrophones were analyzed in order to calculate the wavespeed of the s=1, fluid-dominated wave in the pipe.

4.3 Comparison with theory

The real and the imaginary components of the measured and predicted wavenumbers are shown in Figures 6a and 6b. Three predictions are included using the pipe and soil properties given in Tables 3 and 4: the theory from [17] (equation 25) in which the surrounding soil is treated as a fluid supporting two waves (using the low-temperature pipe wall modulus); the present theory incorporating the full effects of shear (using the room-temperature pipe wall modulus); and the present theory incorporating the full effects of shear (using the low-temperature pipe wall modulus).

Table 3 MDPE pipe properties

(figure in parentheses indicates low-temperature value)

Properties	Pipe
Pipe wall mean radius (m)	84.5×10^{-3}
Pipe wall thickness (m)	11×10^{-3}
Elastic modulus (N/m^2)	1.6 (2.0) x 10^9

Density (kg/m^3)	900
Poisson's ratio	0.4
Material loss factor	0.06
Plate compressional wavespeed (m/s)	1455

1

2 Table 4 Soil and fluid properties

3 (properties of loose unsaturated sand from [26])

Properties	Soil	Water
Bulk modulus (N/m^2)	4.0x10^7	2.25×10^9
Shear modulus (N/m^2)	1.5x10^7	—
Density (kg/m^3)	1500	1000
Compressional wavespeed (m/s)	200	1500
Shear wavespeed (m/s)	100	—

4

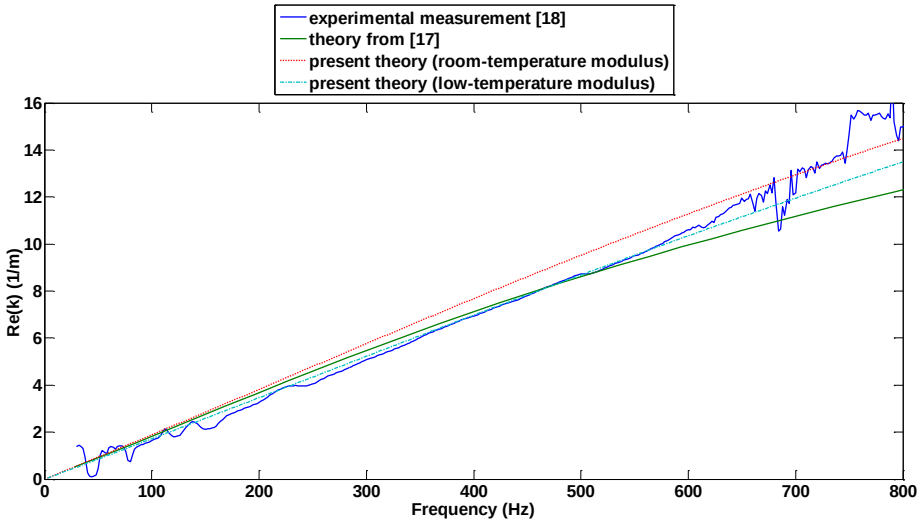

5

6 (a)

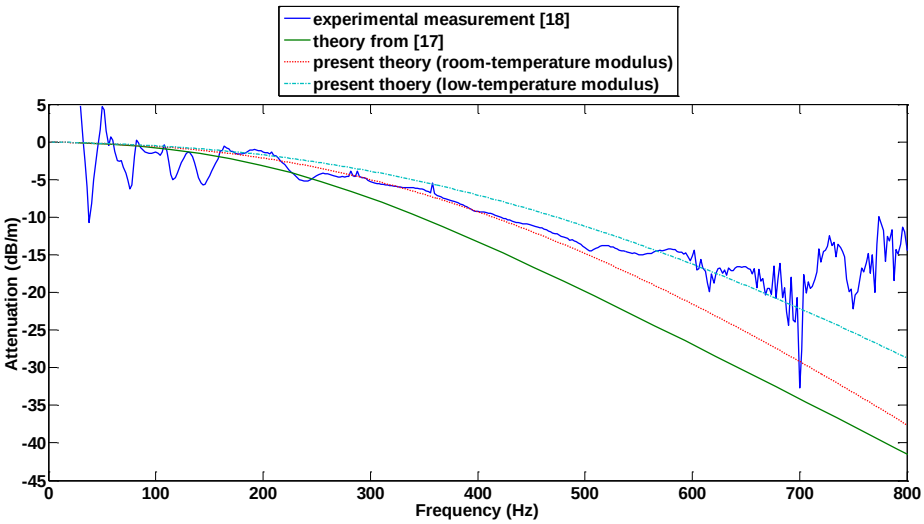

(b)

Figure 6

Measured and predicted wavenumber for *s*=1wave in buried MDPE pipe

(a) Real part; (b) Attenuation (dB/m)

Figure 6a shows that there is good agreement between the measured and predicted values for the real part of the wavenumber at the lower frequencies (<200Hz), whichever prediction is employed; at the mid frequencies (>300Hz and <500Hz) both theories using the low-temperature pipe wall modulus agree well with the measurements; at the higher frequencies shown (>500Hz), the present theory, using either value for the elastic modulus, can be seen to be superior to that given in [17]. In [18] no satisfactory explanation was offered as to the reason for the fall-off in the prediction when compared with the experimental measurements. It is now clear that it was because the effects of shear were not accounted for properly previously, but now are. Regarding the two present predictions, the temperature of the soil was not known on the day the measurement were made but it is likely that the actual value of the pipe wall elastic modulus lay somewhere between the two tabulated values shown.

Figure 6b also shows good agreement between the present predictions and the experimental measurements. Above 600-700Hz the measured data becomes increasingly erratic and, therefore, unreliable. As for the real part of the wavenumber, the agreement between theory and measurement is improved compared with the previous theory given in [17]. In [18] it was suggested that the most likely reason for the discrepancies between theory and experiment was the lack of the ground surface in the theoretical model. This (slightly tenuous) suggestion is no longer required as, as for the real part of the wavenumber, the measurement falls between the two present predictions.

6. Conclusions

In this paper, axisymmetric waves in a fluid-filled, plastic pipe, surrounded by an infinite elastic medium which can sustain both longitudinal and shear waves have been studied. At the pipe/soil interface, one of two possible extreme coupling cases has been considered: the “slip” condition, in which there is lubricated contact between the pipe and the surrounding soil, and no accompanying shear stress.

Analytical expressions have been derived for two wave types: the s=1 wave which is predominantly a fluid-borne wave; and the s=2 wave which predominantly exists in the pipe wall. The real part of the wavenumbers provides information about the wavespeed of the wave, whilst the imaginary part relates to the propagation loss. These expressions permitted insights to be gained into the physical mechanisms at play.

For the s=1 wave, the presence of the pipe wall significantly reduces the wavespeed from the freefield value. The effect of the surrounding soil is predominantly to add stiffness, thus slightly increasing the wavespeed, this being

provided by the effects of shear. There also may be attenuation resulting from both shear and compressional waves radiating into the surrounding medium. Compared with the effects of the compliance of the pipe wall, the effects of the surrounding medium on the wavespeed are, in general, small, whereas the effect on the wave attenuation can be considerable. Experimental measurements show good agreement with the predictions and confirm the theoretical findings; the agreement between measurement and theory is significantly improved compared with the buried pipe model presented previously.

The wavespeed of the s=2 wave is largely unaffected by either the contained fluid or the surrounding medium. The attenuation, however, is increased by including the effects of shear.

The findings presented here provide much needed information for the leak detection community on how current leak detection methods might be improved. Furthermore, they pave the way towards the use of more intelligent approaches to the management and, in particular the detection, of buried infrastructure. In general, it is the s=1, predominantly fluid-borne, wave which is of most relevance to leak detection, and which radiates most effectively to the ground surface. Here, it has been shown that a very simple form of the expression for the s=1 wavenumber may be used in order to accurately predict the wavespeed. The fuller formulation, also presented, is required in order to calculate the wave attenuation.

Future work will address the other pipe/soil coupling extreme: the “no slip” condition in which compact contact between the pipe and the surrounding soil is assumed and for which there is continuity of tangential displacement across the boundary.

Acknowledgement

The authors gratefully acknowledge the support provided for this research by EPSRC, China Scholarship Council (No.2009844130) and National Natural Science Foundation of China (No.50905036). Thanks are also due to Dr. Charles Chassaing - his correspondence in relation to [17] was the inspiration for this work - and to Professor Mike Brennan for his insightful comments on the first draft of this paper.

Appendix

Low-frequency Bessel and Hankel function approximations

In this paper, an $e^{i\omega t}$ time dependence has been assumed. Therefore, to represent outgoing waves, decaying to zero at infinity, Hankel functions of the 2nd kind have been used. At low frequencies, when the arguments of the respective Bessel and Hankel functions are much less than unity, the following approximations have been used, derived from [23].

$$\frac{\mathrm{J}_0\left(k_{fs}^r a\right)}{\mathrm{J}_0'\left(k_{fs}^r a\right)} \approx -\frac{2}{k_{fs}^r a}$$

$$\frac{\mathrm{H}_0''\left(k_{ds}^r a\right)}{\mathrm{H}_0'\left(k_{ds}^r a\right)} \approx \frac{-1}{k_{ds}^r a}$$

$$\frac{\mathrm{H}_1'\left(k_{rs}^r a\right)}{\mathrm{H}_1\left(k_{rs}^r a\right)} \approx \frac{-1}{k_{rs}^r a}$$

References

[1] McMahon W., Burtwell M.H. and Evans M. (2005). Minimizing Street Works Disruption: The Real Costs of Street Works to the Utility Industry and Society. *UK Water Industry Research, London, UKWIR Report Number: 05/WM/12/8, ISBN: 1 84057 408 9.*

[2] N. Metje, P.R. Atkins, M.J. Brennan, D.N. Chapman, H.M. Lim, J.M. Muggleton, S.R. Pennock, J. Ratcliffe, M.A. Redfern, C.D.F Rogers, A.J. Saul, Q. Shan, S. Swingler and A.M. Thomas. Mapping the underworld-state-of-the-art review. *Tunnelling and Underground Space Technology, incorporating Trenchless Technology*, 22 (2007), 568-586.

[3] J. M. Muggleton, M. J. Brennan. The design and instrumentation of an experimental rig to investigate acoustic methods for the detection and location of underground piping systems. *Applied Acoustics* 69 (2008), 1101-1107

[4] Royal, A.C.D., Atkins P.R., Brennan, M.J., Chapman, D.N., Chen, H., Cohn, A.G., Foo, K.Y., Goddard, K., Hayes, R., Hao, T., Lewin, P.L., Metje, N., Muggleton, J.M., Naji, A., Orlando, G., Pennock, S.R., Redfern, M.A., Saul, A.J. Swingler, S.G., Wang, P. and Rogers C.D.F. Site Assessment of Multiple-Sensor Approaches for Buried Utility Detection. *International Journal of Geophysics*, Volume 2011, Article ID 496123doi:10.1155/2011/496123

[5] J M Muggleton, M J Brennan & C D F Rogers. Point Vibration Measurements for the Detection of Shallow-Buried Objects. *Tunnelling and Underground Space Technology* (in press, 2012)

[6] M. J. Brennan, Y. Gao, P. F. Joseph. On the relationship between time and frequency domain methods in time delay estimation for leak detection in water distribution pipes. *Journal of Sound and Vibration* 304 (2007), 213-223.

[7] O. Hunaidi, W. T. Chu. Acoustical characteristics of leak signals in water distribution pipes. *Applied Acoustics* 58 (1999), 235-254.

[8] O. Hunaidi, W. T. Chu, A. Wang, W. Guan. Detecting leaks in plastic water distribution pipes, *Journal of the American Water Works Association* 92 (2000), 82-94.

[9] R. J. Pinnington, A. R. Briscoe. Externally applied sensor for axisymmetric waves in a fluid-filled pipe. *Journal of Sound and vibration* 173 (1994), 503-516.

[10] R. Fuller, F. J. Fahy. Characteristics of wave propagation and energy distributions in cylindrical elastic shells filled with fluid. *Journal of Sound and vibration* 81 (1982), 501-518.

[11] Bikash K. Sinha, Thomas J. Plona, Sergio Kostek, and Shu-Kong Chang. Axisymmetric wave propagation in fluid-loaded cylindrical shells. I: Theory. *Journal of the Acoustical Society of America* **92**, 1132 (1992)

[12] A. Safaai-Jazi, C. K. Jen, G. W. Farnell, and J. D. N. Cheeke. Analysis of liquid-core cylindrical acoustic waveguides. *Journal of the Acoustical Society of America* **81**, 1273 (1987)

[13] Joshua E. Greenspon. Vibrations of Thick and Thin Cylindrical Shells Surrounded by Water. *Journal of the Acoustical Society of America* **33**, 1321 (1961)

[14] Joshua E. Greenspon. Axially Symmetric Vibrations of a Thick Cylindrical Shell in an Acoustic Medium. *Journal of the Acoustical Society of America* **32**, 1017 (1960)

[15] A. N. Jette, J. G Parker. Surface displacements accompanying the propagation of acoustic waves within an underground pipe. *Journal of Sound and Vibration* 69 (1980), 265-274.

[16] J. E. White. *Underground Sound: Application of Seismic Waves*. Elsevier Science Ltd (July 1983), New York.

[17] J. M. Muggleton, M. J. Brennan, R. J. Pinnington. Wavenumber prediction of waves in buried pipes for water leak detection. *Journal of Sound and Vibration* 249(5) (2002), 939-954.

[18] J. M. Muggleton, M. J. Brennan, P. W Linford. Axisymmetric wave propagation in fluid-filled pipes: wavenumber measurements *in vacuo* and buried pipes. *Journal of Sound and Vibration* 270(1–2) (2004), 171-90.

[19] J. X. Liu, T. Y. Li, T. G. Liu, J. Yan. Vibration characteristic analysis of buried pipes using the wave propagation approach. *Applied Acoustics* 66 (2005), 353-364.

[20] A. W. Leissa. *Vibrations of Shells*. (1973) Washington, D.C.: Scientific and Technical Information Office, NASA.

[21] P. M. Morse, K. U. Ingard. *Theoretical acoustics*. (1968) New York: McGraw-Hill.

[22] H. Kolsky. *Stresses Waves in Solids*. (1952) New York, Dover publications, INC.

[23] M. Abramowitz, I. A. Stegun. *Handbook of Mathematical Functions*. (1965) New York: Dover publications.

[24] R.J. Pinnington. Feasibility study to investigate the detection of objects buried in the ground. *ISVR Contract Report* 96/05. (1996), Southampton University.

[25] B. Pavlakovic Leaky guided ultrasonic waves in NDT *Ph.D.* T*hesis* (1998), L*ondon* U*niversity*.

[26] J.M. Head, F.M. Jardine, Ground borne vibrations arising from piling, CIRIA Technical Note 142, 1992.